Homogentisic acid induces autophagy alterations leading to chondroptosis in human chondrocytes: Implications in Alkaptonuria

Silvia Galderisi [a], Maria Serena Milella [a], Martina Rossi [a], Vittoria Cicaloni [a,c], Ranieri Rossi [a], Daniela Giustarini [a], Ottavia Spiga [a], Laura Tinti [c], Laura Salvini [c], Cristina Tinti [c], Daniela Braconi [a], Lia Millucci [a], Pietro Lupetti [b], Filippo Prischi [d], Giulia Bernardini [a], Annalisa Santucci [a]

[a] Department of Biotechnology, Chemistry and Pharmacy, University of Siena, 53100, Siena, Italy
[b] Department of Life Sciences, University of Siena, 53100, Siena, Italy
[c] Toscana Life Sciences Foundation, 53100, Siena, Italy
[d] School of Biological Sciences, University of Essex, Wivenhoe Park, Colchester, CO4 3SQ, UK

Abstract

Alkaptonuria (AKU) is an ultra-rare genetic disease caused by a deficient activity of the enzyme homogentisate 1,2-dioxygenase (HGD) leading to the accumulation of homogentisic acid (HGA) on connective tissues. Even though AKU is a multi-systemic disease, osteoarticular cartilage is the most affected system and the most damaged tissue by the disease. In chondrocytes, HGA causes oxidative stress dysfunctions, which induce a series of not fully characterized cellular responses. In this study, we used a human chondrocytic cell line as an AKU model to evaluate, for the first time, the effect of HGA on autophagy, the main homeostasis system in articular cartilage. Cells responded timely to HGA treatment with an increase in autophagy as a mechanism of protection. In a chronic state, HGA-induced oxidative stress decreased autophagy, and chondrocytes, unable to restore balance, activated the chondroptosis pathway. This decrease in autophagy also correlated with the accumulation of ochronotic pigment, a hallmark of AKU. Our data suggest new perspectives for understanding AKU and a mechanistic model that rationalizes the damaging role of HGA.

Keywords

Alkaptonuria
Homogentisic acid
Autophagy
Apoptosis
Oxidative stress

Silvia Galderisi, Maria Serena Milella, Martina Rossi, Vittoria Cicaloni, Ranieri Rossi, Daniela Giustarini, Ottavia Spiga, Laura Tinti, Laura Salvini, Cristina Tinti, Daniela Braconi, Lia Millucci, Pietro Lupetti, Filippo Prischi, Giulia Bernardini, Annalisa Santucci (2022). Homogentisic acid induces autophagy alterations leading to chondroptosis in human chondrocytes: Implications in Alkaptonuria. Archives of Biochemistry and Biophysics 717, 109137, https://doi.org/10.1016/j.abb.2022.109137.

1. Introduction

Alkaptonuria (AKU) is an ultra-rare autosomal recessive metabolic disease caused by mutations on the homogentisate 1,2-dioxygenase (HGD) gene [1]. These mutations cause loss of function of HGD [2], a cytosolic enzyme involved in the oxidation of homogentisic acid (HGA) to maleylacetoacetate acid in the degradative pathway of the amino acids tyrosine and phenylalanine. Defective HGD activity causes the accumulation of HGA in connective tissues, leading to a black pigmentation typical of alkaptonuric disease. This pigmentation, known with the term “ochronosis”, affects mostly the osteoarticular system (cartilage, bone, synovia and tendons) causing tissue degeneration, chronic inflammation, and ochronotic arthropathy [3]. Alkaptonuric cells, like chondrocytes and synoviocytes, also have intracellular ochronotic pigment [8] included into smooth membrane vesicles in the cytoplasm [9]. Comprehensive analysis has shown that AKU is a multisystemic disease [7] with ochronotic deposition detected in the majority of the body tissues causing organ damage and dysfunction [3–7]. In fact, ochronosis is concomitant with the production of free radical species causing tissue oxidative damage and degeneration [13,14].

Cartilage is one of the most damaged tissues in AKU [15], due to alterations in the structure and in the functionality of AKU chondrocytes that are characterized by aberrant cytoskeleton proteins expression [10], HGA-induced oxidative stress related dysfunctions [13,15,16], reduction of primary cilia length and alteration of Hedgehog signaling [17,18]. Additionally, HGA-induced chondroptosis (a particular form of apoptosis) occurs in AKU chondrocytes causing cell morphologic changes [19]. AKU has been also linked to secondary amyloidosis [10, 11] and angiogenesis [12]. In fact, recent studies have shown that in AKU and HGA treated chondrocytes ochronotic pigment colocalized with SAA-amyloid [12,20].

Autophagy is one of the processes allowing to maintain the homeostasis of articular cartilage and consequently its functionality [21]. Autophagy also allows to balance energy during critical periods of stress and damage, such as during nutrient deprivation [22]. Chondrocytes are the only resident cells in the articular cartilage and they are necessary for the synthesis and the turnover of extracellular matrix. Since articular cartilage is a post-mitotic tissue, the proliferation rate of its cells is very slow with low metabolic turnover [23,24]. Cartilage is an avascular tissue, therefore low levels of nutrients are available for chondrocytes. For this reason, in cartilage cells the autophagy process plays crucial roles in housekeeping physiological processes through the intracellular clearance of unnecessary proteins, pathogens and damaged organelles. Alteration of the autophagic process could lead to the loss of cytoprotective effects in cartilage and, therefore, the occurrence of different diseases, such as osteoarthritis (OA) in which a decrease in the autophagic phenomena occurs [25].

Here we show that HGA causes a state of oxidative stress that over time decreases the protective autophagic process, leading to chondroptosis. We also observed a concomitant HGA-induced block of autophagy and accumulation of ochronotic pigment, which recapitulates AKU physiopathology features.

2. Materials and methods

2.1. Cells culture and treatments

Immortalized human chondrocytes cell line C20 [28] was cultured at 37°C in a humidified atmosphere of 5% CO_2 in DMEM/Ham's F-12 and 10% FBS, 1% P/S and 1% of L-Glutamine.

Alkaptonuric tissue and chondrocytes were obtained from articular cartilage of AKU patients who underwent surgery for total knee replacement. All the procedures were in accordance with the ethical standards of the responsible committee on human experimentation (Comitato Etico Policlinico Universitario di Siena, number GGP10058, date July 21, 2010) and with the Declaration of Helsinki, 1975, as revised in 2000. Informed consent was obtained from all patients. Chondrocytes were isolated by sequential enzymatic digestion: 30 min with 0.1% hyaluronidase, 1 h with 0.5% pronase, and 1 h with 0.2% collagenase at 37 ◦C in wash solution (DMEM + penicillin/streptomycin solution + amphotericin B). AKU cartilage and cells were cultured in DMEM and 10% FBS, 1% P/S and 1% of L-Glutamine and incubated at 37 ◦C in a humidified atmosphere of 5% CO2 95% air. The medium was changed every two days.

10 mM HGA stock solution was prepared by dissolving HGA (Sigma Aldrich) in deionized water. The stock solution was diluted in the cell culture medium reaching the concentrations of 0.033 mM, 0.066 mM, 0.1 mM, 0.33 mM and 1 mM, values which included the HGA range observed in AKU patients [29]. Among these, the treatment with a concentration of 0.1 mM for 2 week was chosen for the next experiments. The concentration of HGA was selected according to cell viability and the appearance of ochronotic pigment, evaluated with Schmorl's staining. The viability of C20 cells after HGA treatment was evaluated through the Muse Count et Viability Kit (Millipore) according to manufacturer instructions. Briefly the differentiation between viable and non-viable cells is based on their permeability to two DNA binding dyes.

Bafilomycin A1 (Baf) solution (Santa Cruz) was prepared after solubilization in DMSO (dimethyl sulfoxide) and diluted in cell culture medium to reach the concentration of 100 nM, 200 nM, and 400 nM. The treatment was maintained in cells for 1 h, 2 h and 3 h. For the analysis of the autophagic flux, the concentration that led to the total blocking of the autophagosomal degradation was used for the experiment. For the simulation of starvation condition was used Hank's Balanced Salt Solution (HBSS). Starvation is a powerful inductor of autophagy and it was used to set positive control condition. First the maximum autophagic response to starvation was evaluated with HBSS treatment for 30 min, 1 h, 3 h and 4 h. As positive control was starvation was induced for 3 h.

For short-time treatment, C20 cells were treated with HGA 0.1 mM for 1 h and 3 h. For the evaluation of the autophagic flux cells were treated with HBSS (Starv), HGA 0.1 mM, Baf 400 nM, Baf 400 nM + HGA 0.1 mM (Baf + HGA) for 3 h. The long-time treatment was carried out treating C20 cells with HGA 0.1 mM for 1 week and 2 weeks. The medium, supplemented with HGA, was changed every 2 days.

2.2. Western blot analysis

Cells at 75–80% confluence were treated as reported above. After treatment, cells were washed with sterile PBS and cellular lysate was prepared with RIPA buffer (Radio immunoprecipitation assay buffer), containing phosphate and protease inhibitors, after disruption by sonication for 7 min in ice bath. The protein concentration was quantified by bicinchoninic acid (BCA) protein assay.

30 µg of protein were separated by 12% sodium dodecyl sulfate-polyacrylamide gel by electrophoresis (SDS–PAGE) and transferred on nitrocellulose membrane.

The primary antibodies used included: anti-Rabbit LC3 (Novusbio, LC3B Antibody, 1:1000), anti-Cytochrome C (Genetex 1:1000), anti-NDUFV1 (Genetex, 1:1000), anti-BCL-2 (Santa Cruz, 1:500), anti SQSTM1/P62 (Genetex 1:1000) and anti-GAPDH HRP-conjugated (Sigma-Aldrich, Anti-GAPDH, 1:50.000). The secondary antibody was an anti-rabbit HRP-conjugated antibody (Sigma-Aldrich, Anti-rabbit IgG, 1:80000). The immunoreactive bands were detected using ECL (Luminata Crescendo, Merck Millipore) and images acquired by LAS4000 machine (GE Healthcare). Protein levels were normalized against GAPDH (Glyceraldehyde 3-phosphate dehydrogenase), used as a protein-loading control.

2.3. Immuno-fluorescence microscopy

Cells were seeded in sterile chamber slides at a density of 4·104 cells for C20 cells. After treatments, they were washed with PBS and fixed with methanol for 20 min at 20 ◦C and acetone for 5 min at 20 ◦C. The blocking procedure was carried out with NGS 5% in PBS-BSA 1% and incubated in wet room for 20 min. The anti LC3B antibody (Novusbio, LC3B Antibody) was diluted to 1:200 in NGS 1%, PBS-BSA 0.1% and incubated overnight at 4 ◦C. After three washes in PBS for 10 min, cells were incubated with the secondary antibody goat anti-rabbit (Alexa Fluor 488 goat anti-rabbit IgG) in NGS 1%+PBS-BSA 0.1% and incubated in a dark wet room for 1 h. After three washes with PBS, nuclei were stained DAPI (Abcam) for 5 min. Samples were visualized by fluorescence microscopy (Zeiss AxioLabA1). Fluorescence intensity quantification was carried out with ImageJ software.

2.4. Evaluation of oxidative stress

The free thiol groups were measured on protein extracts using Ellman's reagent (5,5′ -dithiobis-(2-nitrobenzoic acid), DTNB) [14]. Thiol groups in the samples react with Ellman's reagent producing 2-nitro-5--thiobenzoate (NTB) with an absorbance of 412 nm, directly proportional to the concentration of thiol groups.

2.5. Transmission electron microscopy (TEM)

Alkaptonuric tissue and chondrocytes were fixed in 2.5% glutaraldehyde in 0.1 M sodium cacodylate (pH 7.4) containing 2% tannin and post-fixed in 1% osmium tetroxide dehydrated in ethanol and embedded in epoxy resin. Samples were examined in a transmission electron microscope (100CX II, JEOL, Peabody, MA) operated at 80 kV.

2.6. Nuclear staining with 4', 6-diamidine phenylindole (DAPI)

C20 cells were seeded in sterile chamber slides and, after treatment, they were washed in PBS and fixed in 70% ethanol for 30 min. Finally, the slides were rinsed with PBS for two times and mounted with fluoroshield mounting medium with DAPI (Abcam, ab104139). Images were acquired by fluorescence microscopy (Zeiss AxioLabA1).

2.7. Detection and quantification of ochronotic pigment

C20 cells were seeded in sterile chamber slides and, after treatment period, the ochronotic pigment formation was detected by two different methods: the Schmorl's staining and formaldehyde-induced fluorescence. In the first case, chamber slides were washed in PBS twice, fixed in ethanol 75% and stained with Schmorl's staining solution [29–31]. Nuclei were counterstained with nuclear fast red solution. Cells were washed deeply in deionized water and dehydrated with crescent concentrations of ethanol. After complete drying, samples were submerged in xylene and mounted with Eukitt mounting medium (Sigma-Aldrich). Stained samples were observed under bright-field microscope. The intensity of blue pigmentation was quantified, for each cell, with the function Measure of ImageJ software, and the values obtained were normalized with area.

For the pigment detection with fluorescence [32], after treatment, cells were washed in PBS and fixed in PFA 4% for 10 min, then the slides were washed in water and mounted with Fluoroshield mounting medium (Abcam). Images were obtained with Zeiss AxioLabA1 fluorescence microscope in FITC filter. Fluorescence intensity quantification was carried out with ImageJ software.

2.8. Statistical analysis

All the experiments are expressed as mean ± SD. ANOVA tests were used for the evaluation of differences between data. Data were analyzed by one-way analysis of variance with post hoc Tukey's multiple comparisons. Differences of $P < 0.05$ were considered significant and identified with asterisks in graphs.

2.9. Shotgun proteomics

After 2 weeks of HGA treatment, chondrocytes cells were washed twice with sterile PBS and lysed in RIPA buffer with protease and phosphatase inhibitors. Protein content in cell lysates was evaluated with the BCA assay. The enzymatic digestion protocol was based on FASP technique [33]. A volume equal to 100 µg of proteins for every sample were mixed with a solution of 8 M urea in 100 mM Tris HCl at pH 8.5 in the presence of 0.1 M DTT. The solutions were then incubated at room temperature for 30 min. After disulphide bond reduction, samples were transferred into the ultrafiltration units (Amicon Ultra-0.5 ml 10 kDa, Millipore) and centrifuged at 13,800 g for 30 min. For the alkylation, 200 µl of 0.05 M iodoacetamide IAA (Sigma Aldrich) in 8 M urea pH 8.5 were added to every sample and each mixture was incubated for 20 min at the dark. Filter units were centrifuged at 13,800 g for 20 min, and then four washes were performed: the first two adding 100 µl of 8 M urea pH 8.5 to the filter, and the remaining two using 100 µl of 50 mM Ammonium Bicarbonate. Protein digestion was performed overnight at 37 ◦C adding 4 µg of trypsin. Filtered tryptic peptides were collected in a new tube, and the filters were washed with 100 µl of 0.1% formic acid.

Digested samples were desalted using OASIS cartridges (Waters), dried and reconstituted in 97% water, 3% acetonitrile and 0.1% formic acid. LC-MS/MS measurements were carried out using Q-Exactive Plus- Orbitrap mass spectrometer (Thermo Scientific). The peptide separation was performed at 50 ◦C using an Acquity UPLCTM peptide CSH C18 column, 1 mM × 100 mM, 1,7 µm, 130 Å (Waters) at a flow rate of 100 µl/min using a 230-min gradient from 3% to 90% eluent B (acetonitrile plus 0.1% formic acid) in eluent A (water with 0.1% formic acid). The mass spectrometer was set up in a data-dependent acquisition (DDA) mode in which the most intense ions, a maximum of twelve in this kind of experiments, from a full MS scan spectrum (200–2000 m/z) were selected for fragmentation. Protein identification was performed using Proteome Discover (Thermo Scientific) and Sequest as the protein database. A false discovery rate (FDR) correction of 1% was applied to the identified peptides to enhance the confidence level of identified proteins.

The output of a proteome analysis is typically a long list of identified factors that have a probability score and an associated quantitative value. In order to understand and decipher these data and to generate testable hypothesis, the list has to be further classified and filtered. Functional annotation analysis was carried out using DAVID 6.8 [34] and FunRich 3.1.3 [35] analytic tools aimed at systematically extracting biological meaning from large gene/protein lists. For every pathway, we calculated the percentage of involved genes, fold enrichment and p-value (Hypergeometric test) in order to evaluate significance of an association between the two kinds of categorical classification for a set of objects (for example, presence of a protein in the list of interest and its belonging to a pathway or any other ontology term). In the case of enrichment analysis, the intersection between a protein list of interest and a list of proteins involved in a certain pathway is calculated. The estimated probability that a gene set with a given enrichment score (normalized for gene set size) was settled with p value < 0.05. FDR, estimated probability that a gene set with a given enrichment score (normalized for gene set size) was settled p value < 0.05. For a functional interpretation of the results, the protein identifiers are associated to its related Gene Ontology (GO) terms [36] overcoming the redundancy in terminology for “biological process”, “molecular function” or “cellular component” [37].

2.9.1. emPAI protocol for quantitation

To estimate absolute protein contents in complex mixtures, we previously defined a protein abundance index (PAI) [38]:

PAI= ***Number of observed peptides/ Number of observable peptides***

Where “**Number of observed peptides**” is the number of experimentally observed peptides and “**Number of observable peptides**” is the calculated number of observable peptides for each protein. The Exponentially Modified Protein Abundance Index (emPAI) is easily calculated starting from PAI value and it is defined as:

emPAI = 10PAI-1

It offers an approximate, label-free, relative quantitation of the proteins in a mixture based on protein coverage by the peptide matches in a database search result. Generally, it is applied to comprehensive protein expression analysis adding important quantitation

information to proteomic experiments. However, it is not a consistent measure across various samples. As a matter of the fact, each proteins individual emPAI was normalized to the total emPAI of that set [39]. Fold change ratios for identified proteins based on normalized emPAI values of treatment and control were calculated. We selected a cutoff for biological significance of fold change which is < 0.5 for downregulated proteins and >1.5 for the upregulated [39].

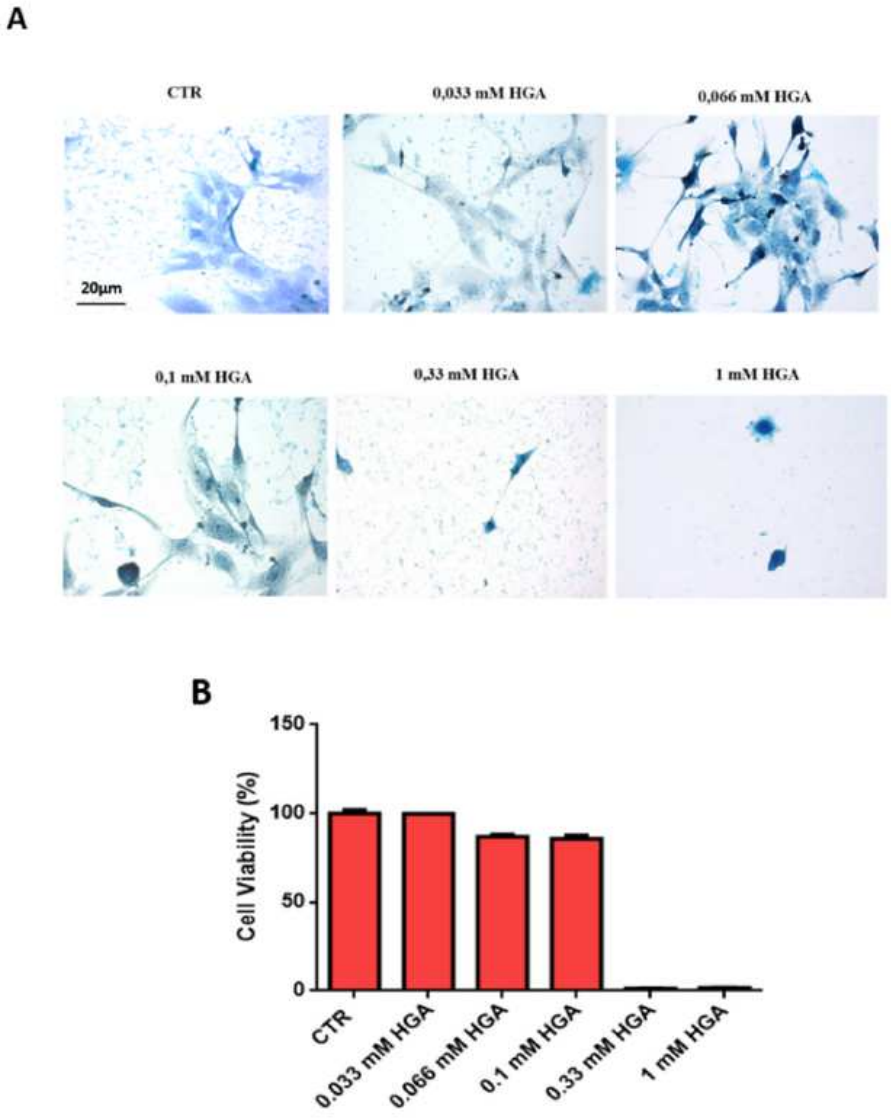

Fig. 1. A) HGA effect on C20 ochronotic pigment production. Evaluation of pigment formation with Schmorl's staining following supplementation of increasing HGA dosages. B) C20 cell viability following increasing doses of HGA.

3. Results

3.1. Selection of HGA treatment concentration

The optimal HGA concentration to be supplemented for the set up at C20 AKU model was evaluated according to ochronotic pigment deposition by Schmorl's staining. 0.033–1 mM range HGA concentration was tested for 2 weeks. HGA 0.1 mM concentration was selected for following experiments, since it produced evident pigmentation (Fig. 1A) while allowing

high cell viability (Fig. 1B), confirming previous data obtained in primary human cells [40]. Cell dimorphism was observable in HGA-treated cells, even at low HGA concentrations, in the range of HGA plasma levels in AKU patients.

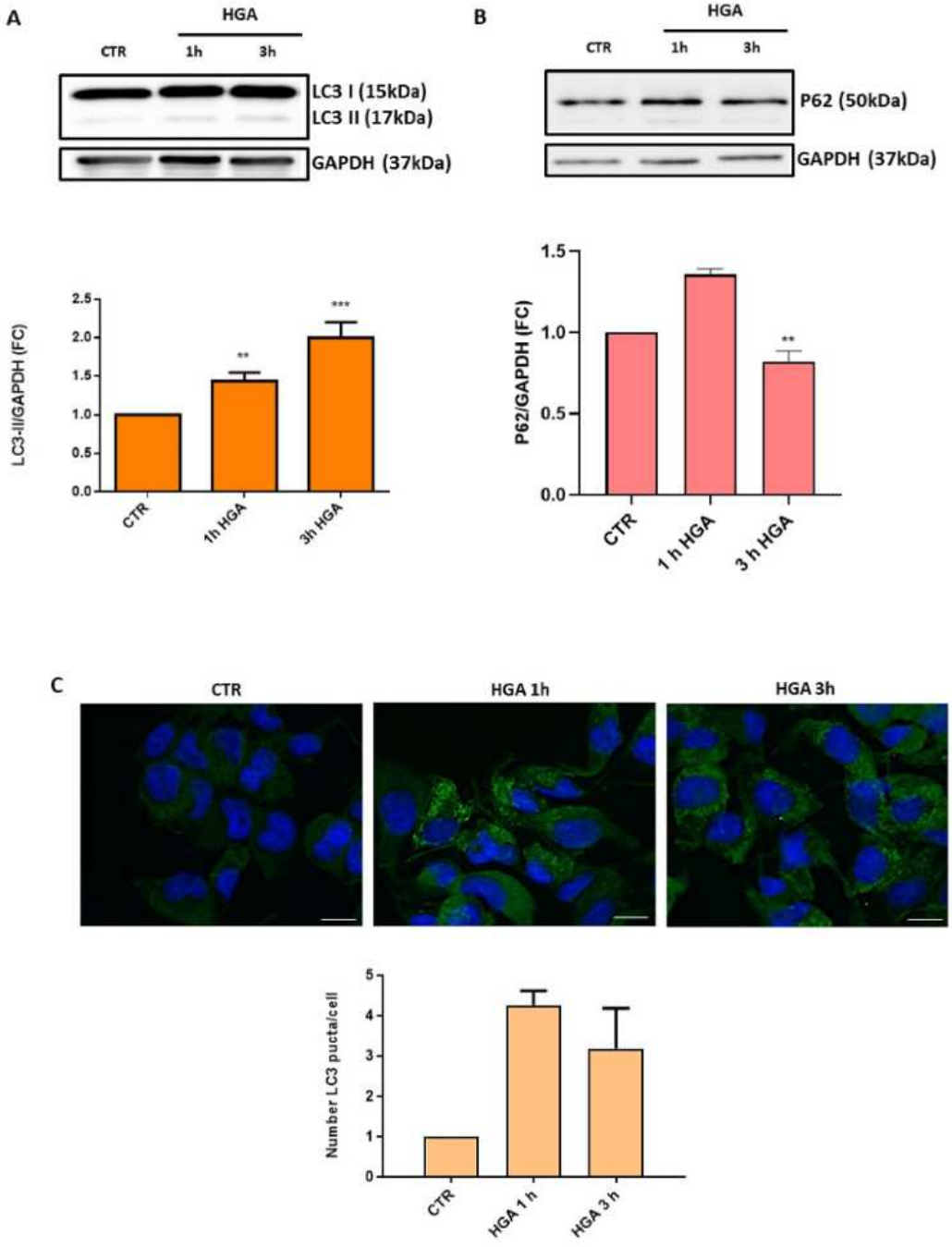

Fig. 2. HGA effect on C20 autophagy. A) Upper panel: western blotting of LC3-I and LC3-II and GAPDH. Lower panel: quantification of the increase of LC3-II after 1 h and 3 h of HGA 0.1 mM treatment. The ratio between band volume of LC3-II over band volume of GAPDH is reported in fold change. B) Upper panels: Western blotting of P62 and GAPDH. Lower panel: quantification of P62. The ratio between band volume of P62 over band volume of GAPDH is reported in fold change. C) Upper panel: detection of LC3 fluorescent puncta (green) in C20 cells after treatments. Cell nuclei were stained with DAPI (blue). Cells are shown at x40 magnification. Scale bar = 20 μm. Lower panel: numer of LC3 punta normalized with the number of cells. (For interpretation of the references to color in this figure legend, the reader is referred to the Web version of this article.)

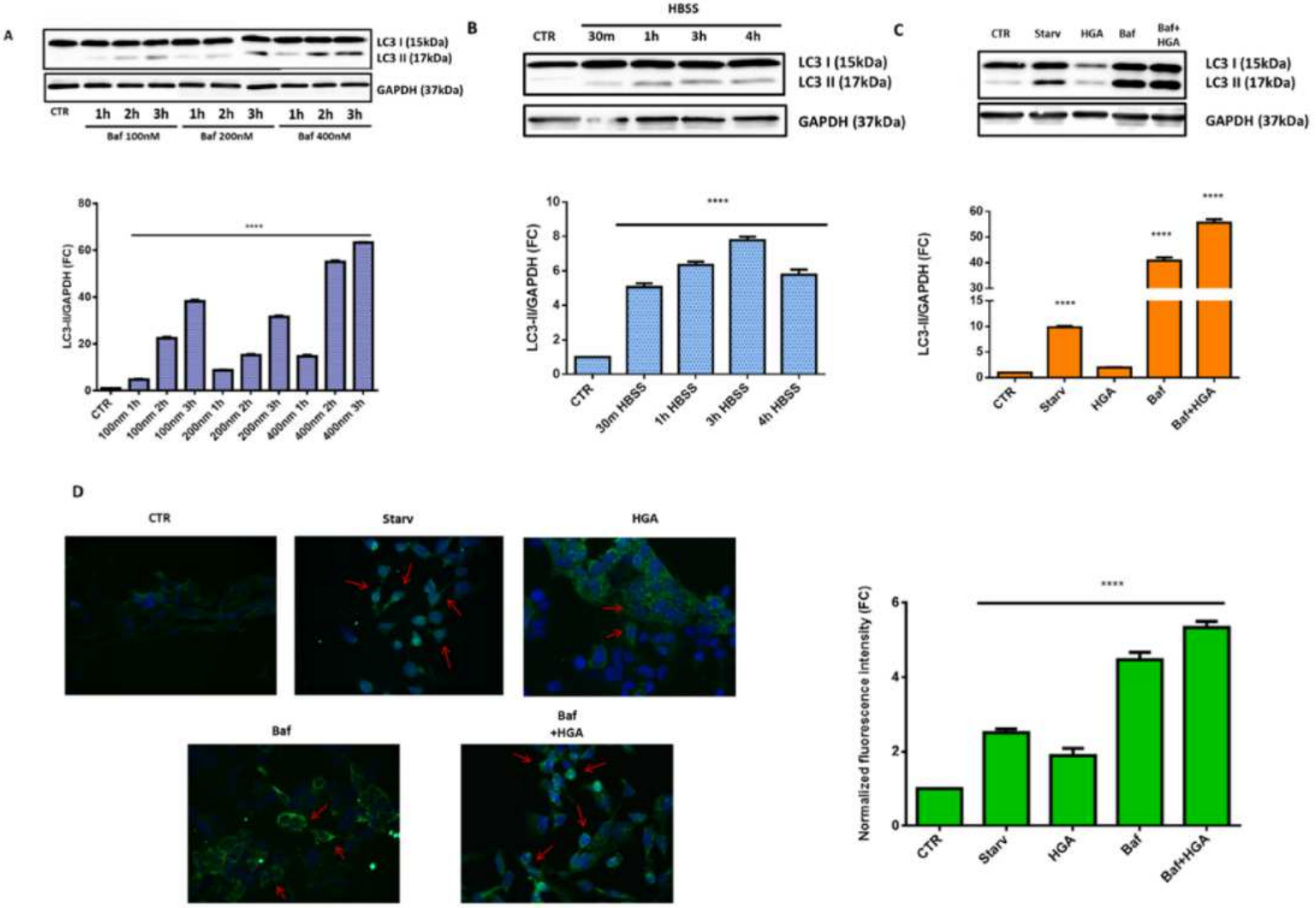

Fig. 3. Evaluation of autophagic flux following 0.1 mM HGA treatment of C20 cells. A) Baf treatment. Upper panel: western blotting of LC3-I and LC3-II and GAPDH after Baf treatment. Lower panel: quantification of the increase of LC3-II after increasing concentrations and times of C20 cells treatment with Baf. B) HBSS treatment. Upper panel: western blotting image of LC3-I and LC3-II and GAPDH after HBSS treatment. Lower panel: increase in the amount of LC3-II following 3 h of HBSS treatment. C) Upper panel: western blotting bands of C20 LC3-I and LC3-II and GAPDH. Lower panel: quantification of LC3-II protein in C20 after treatment with HBSS for 3 h, under starvation conditions (Starv) and treatments with HGA 0.1 mM for 3 h (HGA), Baf 400 nM for 3 h and Baf 400 nm + HGA 0.1 mM for 3 h (Baf + HGA). For all western blotting analysis, the ratio between band volume of LC3-II over band volume of GAPDH is reported in fold change. D) Left panel: detection of cellular localization of LC3 protein in C20 cells after treatment. Red arrows indicate the increment in LC3 puncta number (in green) after treatments. Cell nuclei were stained with DAPI (blue). Cells are shown at x40 magnification. Right panel: quantitative analysis of intensity of LC3 normalized with area of the cells and reported as fold change. (For interpretation of the references to color in this figure legend, the reader is referred to the Web version of this article.)

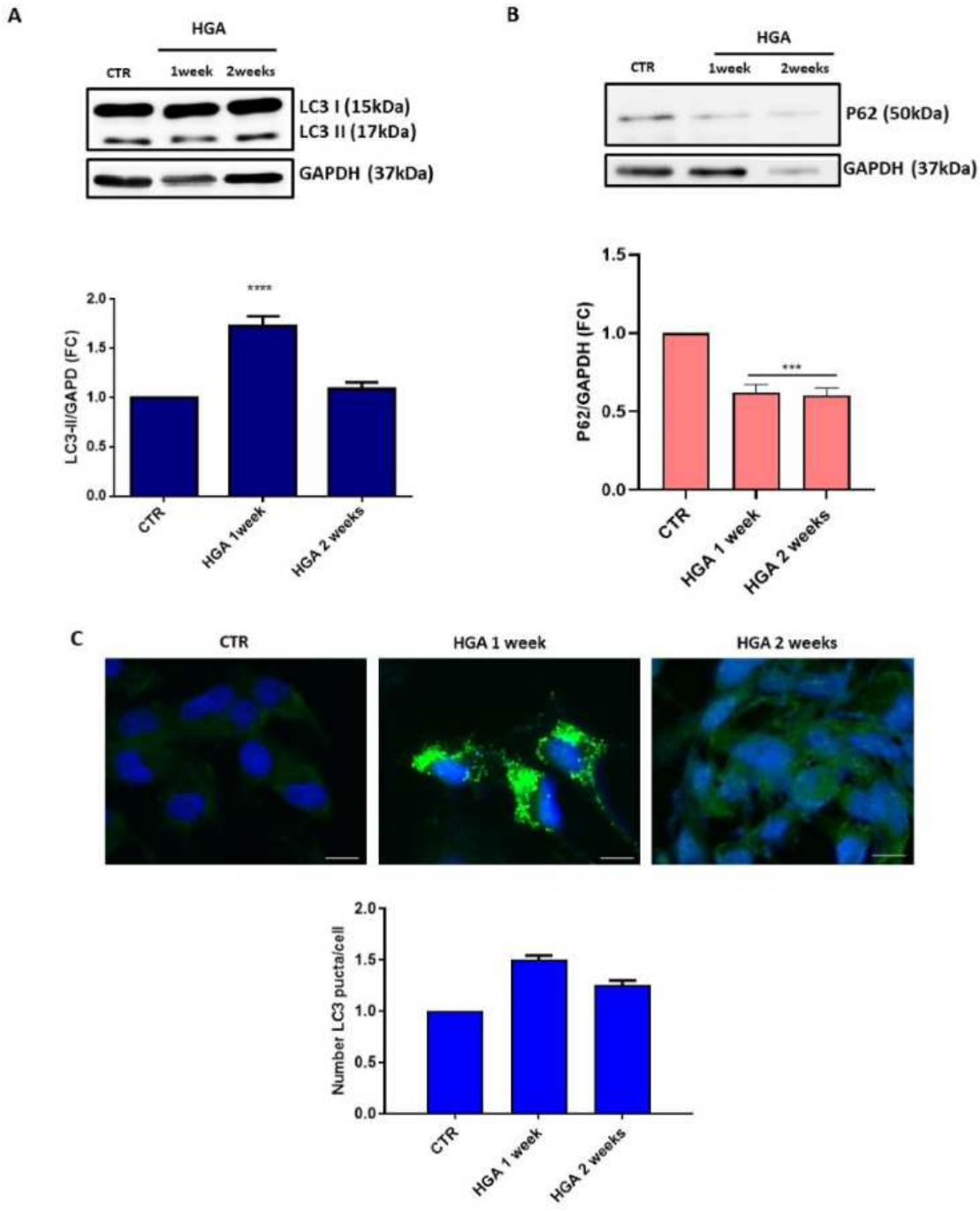

Fig. 4. Autophagic C20 response to LC3 long term (1–2weeks) HGA treatment. A) Upper panel: Western blotting of LC3-I and LC3-II and GAPDH. Lower panel: quantification of LC3-II. The ratio between band volume of LC3-II over band volume of GAPDH is reported in fold change. B) Upper panels: Western blotting of P62 and GAPDH. Lower panel: quantification of P62. The ratio between band volume of P62 over band volume of GAPDH is reported in fold change. C) Upper panel: detection of LC3 fluorescent puncta (green) in C20 cells after treatments. Cell nuclei were stained with DAPI (blue). Cells are shown at x40 magnification. Scale bar = 20 μm. Lower panel: numer of LC3 punta normalized with the number of cells. (For interpretation of the references to color in this figure legend, the reader is referred to the Web version of this article.)

3.2. HGA-induced autophagy alteration

In order to evaluate the HGA influence on the autophagic activity, protein extracts of C20 cells, treated with HGA 0.1 mM, were submitted to western blotting analysis to determine the production of LC3-II protein, an indicator of autophagosome formation. As shown in Fig. 2A, an alteration of the autophagy process was deduced by the increase in the amount of LC3-II protein following HGA treatment. A time-dependent effect of HGA on the quantity of

LC3-II could be noticed, since the protein amount was higher after 3 h (2.01 ± 0.21 fold) respect to 1 h (1.44 ± 0.11 fold) of treatment.

Along with the LC3-II levels determination, it had been also analyzed the degradation of the P62 protein. Indeed, P62 is strictly connected with the autophagic pathway, since it has an essential role in the ubiquitinated proteins formation: P62 recognize toxic cellular wastes, enabling their autophagic degradation. The intracellular level of P62 is modulated by several signals, in particular is regulated at transcriptional level by oxidative stress, while at post-translational level by autophagic degradation. HGA treatment caused in chondrocytes the immediate onset of oxidative stress and inflammation, that induced in cells the activation of several pathways as a defence response. Among others, oxidative stress and inflammation activated P62 synthesis [79] and oxidation [80]. Indeed P62 is positively regulated by oxidative stress, but at the same time it represents a key factor for the autophagic flux [81]. Thereby, immediately after HGA treatment (1 h), the effect of oxidative stress was visible on the P62 transcription, that increased, and on the activation of autophagy. The autophagic signal increased over time, with a consequent rising of the autophagic flux and cargo degradation. P62 acts as a substrate of autophagic degradation, carrying ubiquitinated proteins. For this reason, the increase of LC3-II after 3 h of HGA treatment occurred together with the P62 reduction (Fig. 2A and B), demonstrating the activation of the autophagic pathway.

Finally, to verify that the increase of LC3 was associated to the formation of new autophagosomes, we counted the number of LC3 positive puncta through Immunofluorescence. Results confirmed the marked increase of autophagosomes in HGA treated cells, compared to the control (Fig. 2C).

3.3. HGA-induced autophagic flux

The increase in the amount of LC3-II can be linked to the formation of autophagosomes or to a block in autophagosomal maturation and completion of autophagy pathway [41]. An agent that blocks the fusion of autophagosomes with lysosome, Bafilomycin A1, was adopted to distinguish if the increase of LC3-II after HGA treatment was caused by the real induction of autophagy after treatment or if HGA may acts as a blocker of autophagosome degradation. First, we determined the concentration of Bafilomycin A1 that blocked the total autophagosomal degradation, selecting 3 h of treatment at a concentration of 400 nM (Fig. 3A). Then the time of starvation treatment leading to the maximal autophagic response in C20 cells was evaluated. We found that 3 h of treatment with an inductor of starvation condition, HBBS, caused the highest LC3-II expression (Fig. 3B), thus deducing the maximal autophagic response and setting the positive control conditions.

The treatment of C20 with 0.1 mM HGA caused an increment in the amount of LC3-II compared with untreated sample (1.98 ± 0.09 fold; Fig. 3C). Western blotting levels of LC3-II in C20 cells co-treated with Bafilomycin A1 and HGA (Baf + HGA) (55.61 ± 1.31 fold) were higher compared to the treatment with only Bafilomycin A1 (40.79 ± 1.28 fold).

Results from LC3-II immuno-fluorescence assay (Fig. 3D) confirmed LC3 increment in HGA-treated C20 cells, even more evident in cells co-treated with both HGA and Bafilomycin A1 compared to the treatment with Bafilomycin A1 alone.

Taken together, data indicated that HGA acted as an inductor of autophagic flux and not as a blocking agent of autophagosome degradation.

3.4. HGA-induced autophagy alteration after long term treatment

We then evaluated the C20 autophagic long-term response to HGA stimulus. Cells were treated for 1 and 2 weeks with 0.1 mM HGA and LC3-II and P62 expression were quantified by western blotting, while autophagosomes number was quantified with Immunofluorescence against LC3. After 1 week the increase in the marker of the autophagosome was 1.78 ± 0.9 fold, while after a longer period of treatment (2 weeks) we observed a decrease of the marker of 1.09 ± 0.06 fold, suggesting a reduction of autophagic activity back to the control levels (Fig. 4A). The fact that the autophagy pathway was still active after long term HGA treatments was confirmed by the lower level of P62 detected in AKU cell model, compared to the control. Indeed, P62 was degraded with toxic cargo by autophagosomes during the autophagic process (Fig. 4B).

Result was confirmed by the number of LC3 puncta detected, that reached the higher value after 1 week of HGA treatment, and again decreased after 2 weeks of treatment (Fig. 4C).

3.5. HGA-induced oxidative stress

A cause of alteration of autophagic process in C20 cells could be linked to a state of oxidative stress caused by HGA. We then measure the level of oxidative stress caused by HGA action using total thiols and intracellular ROS quantifications. We found that HGA was an inducer of oxidative stress also in C20 cell line, as indicated by the decrease in the amount of free thiols. A time dependent progression of oxidative stress could be also noticed, since the amount of thiols was low after 2 weeks of HGA (Fig. 5).

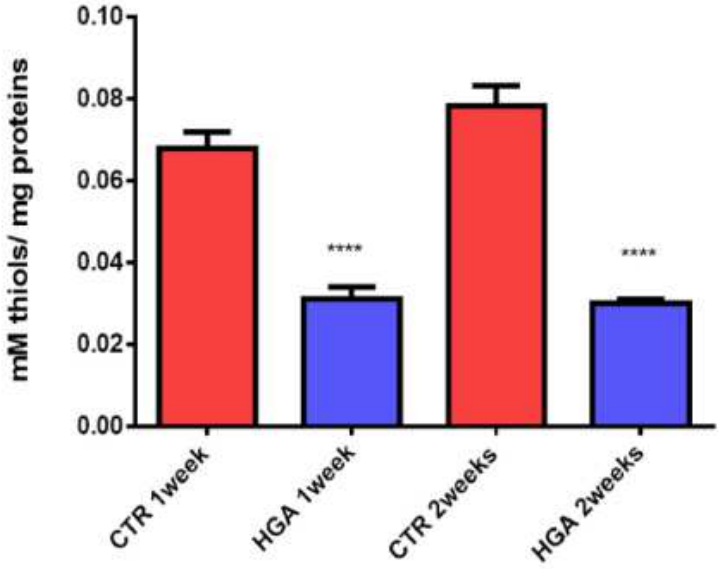

Fig. 5. Induction of oxidative stress in C20 cells after HGA treatment. The graph represents the quantification of protein thiols on µg of protein, calculated by the use of Ellman's reagent on the protein extract. In red are reported thiols from C20 cells without treatment (CTR), in blue thiols from C20 cells treated with HGA 0.1 mM. (For interpretation of the references to color in this figure legend, the reader is referred to the Web version of this article.)

3.6. Mitochondrial damage in AKU chondrocytes and cartilage

HGA could cause a complex damage situation in cells causing a chronic oxidative stress which could lead to dysfunctional mitochondria. Mitochondrial damage was evaluated by TEM analysis of AKU chondrocytes (Fig. 6A,C) and AKU cartilage (Fig. 6B). A non AKU cartilage TEM image is reported in Supplementary Materials 1 (Fig. S1). AKU chondrocytes appeared chondroptotic, characterized by an intense vacuolization, especially those present within AKU cartilage (Fig. 6B). Particularly, both AKU chondrocytes and cartilage were characterized by the presence of the typical autophagosomal vesicles. Mitochondria were swollen with the loss of the internal cristae, characteristics of mitochondrial damage. In AKU cartilage was notable the typical black pigmentation, included in lamellar bodies in AKU chondrocytes.

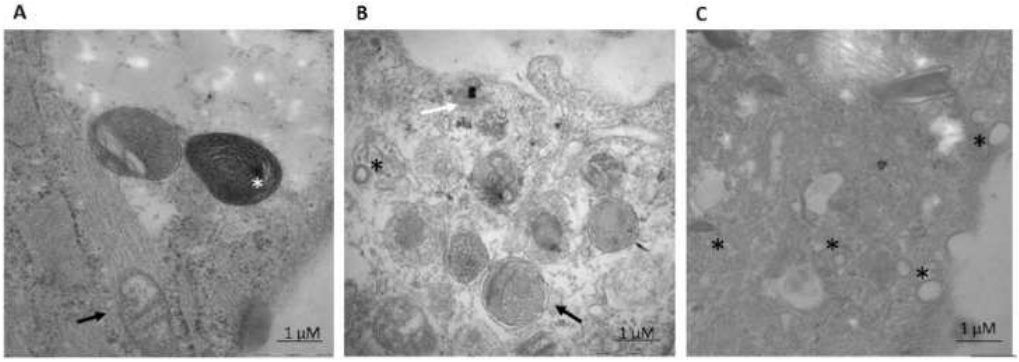

Fig. 6. TEM observation of AKU chondrocytes (A,C) and cartilage (B). Mitochondria are indicated by black arrows. The white arrow shows the black spots of black pigment, hallmark of AKU, located in lamellar bodies (white asterisk). Black asterisks indicate autophagosomal vesicles. Images were taken at 14,000x magnification.

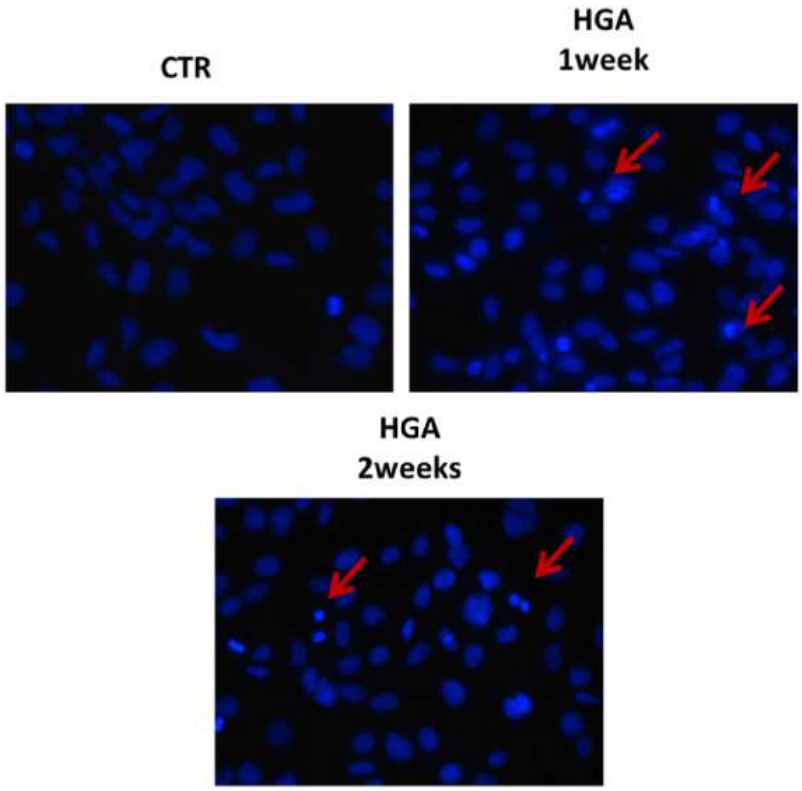

Fig. 7. Assessment of nuclear morphological changes and DNA damage in C20 cells after 0.1 mM HGA treatment for 1week and 2weeks. Cells are shown at x40 magnification. Red arrows indicate nuclear morphology change, considered a biochemical hallmark of chondroptosis. (For interpretation of the references to color in this figure legend, the reader is referred to the Web version of this article.)

3.7. HGA-induced nuclear morphology alteration and chondroptosis

DAPI staining allowed to detect apoptotic nuclei in C20 cells after HGA treatment. As showed in Fig. 7, long time treatment caused an increase in the number of apoptotic cells and a more intense DAPI staining due to the loss of membrane integrity. The alteration of nuclear shape was mainly visible after 1 week and 2 weeks of HGA treatment. Nuclei loss the regular shape and well-defined boundaries compared with control and a chromatin condensation, is visible. This data suggests that HGA treatment act as an apoptosis inducer.

3.8. HGA-induced ochronotic pigment deposition

A hallmark of AKU is the development of an intracellular ochronotic pigment. In order to monitor the pigment deposition over time, HGA treated C20 cells were stained with the melanin-specific Schmorl's staining technique (Fig. 8A). The ochronotic pigment, evidenced by blue [[fig6 & 7]] color spots, was present in the intracellular portion of cells after 1 week and, mostly, after 2 weeks of HGA treatment. Formaldehyde-induced fluorescence was adopted as an additional method for melanin-pigment identification. Formaldehyde fixation induces a pronounced auto-fluorescence of cells which develop the ochronotic pigment (Fig. 8B). Indeed, fluorescence became slightly evident after 1 week of HGA treatment and became significantly higher after 2 weeks.

The quantification of fluorescence intensity revealed a time dependent increase in pigmentation.

3.9. Proteomic analysis in AKU chondrocytes model

A shotgun proteomics approach was performed to further evaluate C20 autophagic long-term response to HGA stimulus. C20 cells were treated for 2 weeks with 0.1 mM HGA and LC-MS/MS analysis was carried out.

The total amount of proteins with high confidence in C20 HGA-treated and untreated (CTR) samples were respectively 2320 and 2482, with 2138 common proteins (Fig. 9) and an overlap index based [[fig 8 fig 9]] on Jaccard coefficient (which measures similarity between finite sample sets and it is defined as the size of the intersection divided by the size of the union of the sample sets) of 0.45.

We performed a functional enrichment analysis of both datasets (for a complete pathways list and the corresponding percentage of involved genes, fold enrichment and p-value (Hypergeometric test) see Supplementary Materials 2). Interestingly, unsupervised clustering of the resulting data distinguished the two C20 samples revealing a diverse protein profile. A comparison between the two datasets was executed showing a difference (p value (Hypergeometric test) < 0.05) in several GO terms related to biological processes, such as mTOR signaling pathway (GO:0031929), p38 MAPK signaling pathway (GO:0038066) and in p53 pathway (GO:0072332), which are all upregulated in HGA-treated sample. mTOR is the main inhibitory signal of autophagy and it is regulated by an array of diverse intracellular and environmental cues, including growth factors, energy levels, nutrient availability and stresses, like oxidative stress [42]. Additionally, apoptotic process (GO:0006915) resulted to be enriched in HGA-treated cells in comparison with

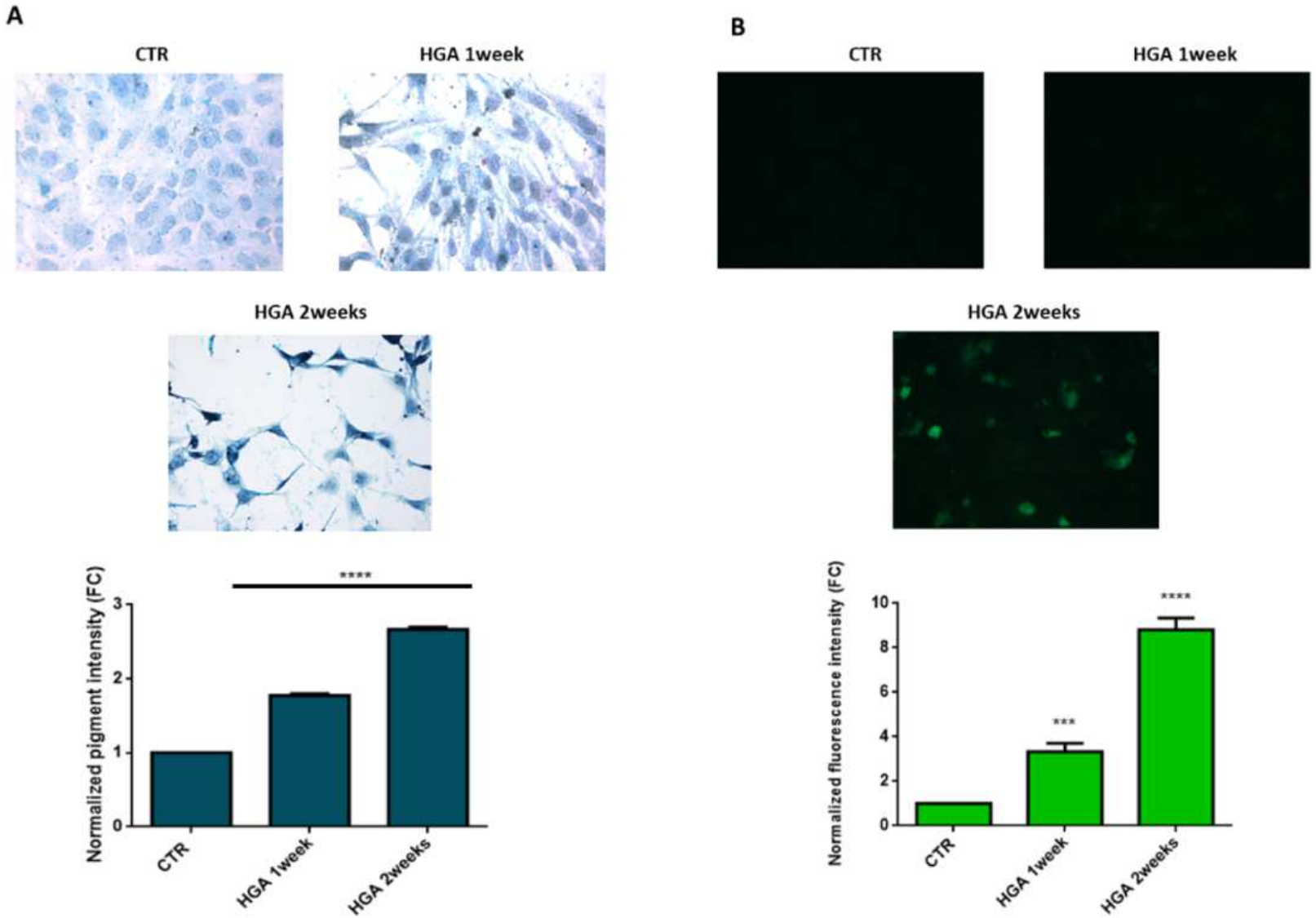

Fig. 8. Detection of time-dependent ochronotic pigment deposition in HGA-treated C20 cells. A) Upper panel: Schmorl's staining, in which the pigment acquired a blue discoloration. Lower panel: quantification of blue pigmentation intensity normalized with area. B) Upper panel: ochronotic pigment detection by formaldehyde fixation. Lower panel: quantitative analysis of fluorescence intensity normalized with area and reported as FC. Cells where treated with HGA 0.1 mM for 1week and 2weeks. Cells are shown at x40 magnification. (For interpretation of the references to color in this figure legend, the reader is referred to the Web version of this article.)

Fig. 9. Venn Diagram. It represents the number of reproducibly quantified proteins for HGA-treated C20 cells (2320 proteins) and CTR C20 cells (2402 proteins); common proteins are 2138 with a Jaccard coefficient of 0.45.

CTR cells. Particularly interesting are three proteins exclusively included in the 182 HGA-treated proteins subgroup such as: Keratin type I cytoskeletal 14 (KRT14), that in association with of cathepsin D and cytokeratin 8 reflects a cellular adaptive response by the autophagy -lysosomal pathway [66], Palmitoyl-protein thioesterase 1 (PPT1) which is one of the target proteins upregulated by transcriptional factor EB (TFEB), the master controller of autophagy and lysosome biogenesis [67–69] and Cytochrome b-c1 complex subunit 8 (UQCRQ), part of the mitochondrial electron transport chain which drives oxidative phosphorylation.

In order to better investigate the up- or down-regulation of proteins involved in the above mentioned biological processes, we calculated the fold change of the normalized EmPAI of the proteins listed in Table 1 (for more details see Supplementary Materials2). We selected a cutoff for biological significance of fold change (FC) which is < 0.5 for down-regulated proteins and >1.5 for the up-regulated.

Shotgun proteomics analysis confirmed a down-regulation of LC3-II upon a longer period (2 weeks) of HGA treatment, confirming a reduction in the autophagic activity. Moreover, in accordance with the study of Ruiz-Romero [43], NDUV1 resulted to be increased in HGA-treated cells. The increased abundance of one of the core subunits of complex I (GO:0005747), NDUV1 may also affect mitochondrial respiratory chain efficiency and, consequently the mitochondrial dysregulation of energy production that takes place in OA disease like AKU [43]. Complex I functions consist of the electrons transfer from NADH to the respiratory chain. It is involved in mitochondrial electron transport, NADH to ubiquinone (GO:0006120) and in response to oxidative stress (GO:0006979).

Similarly, ATP5B is a subunit of mitochondrial membrane ATP synthase, responsible to produce ATP from ADP in the presence of a proton gradient across the membrane which is generated by electron transport complexes of the respiratory chain. Gene knockdown of ATP5B resulted in decreased autophagic flux indicating a role for this protein in the promotion of autophagy [70]. ATP5B, along with HSPE1 and PNP, was also outlined in the study of Wang et al. [71] describing the proteins involved in the autophagy inducted via amino acid starvation. Additionally, several of the proteasome components (such as PSMC5) were among the proteins highly retained by autophagy in starvation [72]. Another

key regulator of autophagy is SNAP29, a critical components of vesicle trafficking and endocytosis that in association with Syx17, is recruited from the ER to regulate the autophagosomes formation [73]. Conversely, GAPDH stimulates autophagy by different pathways. Various conditions exhibit a correlation between autophagy and the translocation of GAPDH in different subcellular compartments, especially to nucleus [74]. In a situation of oxidative stress and inflammation, as occur after HGA treatment, p53 and NO upregulating the mRNA level of GAPDH via an unclear mechanism, enhancing GAPDH nuclear translocation and pro-apoptotic function [75]. PRDX1, PRDX5 and NNT are other proteins linked to oxidative stress. Specifically, PRDX1 plays a role in cell protection against oxidative stress by detoxifying peroxides and as sensor of hydrogen peroxide-mediated signaling events [76], PRDX5 is a mitochondrial dysfunctional – related protein, upregulated in cases of ROS production and oxygen deprivation [77], whereas NNT critically regulates mitochondrial redox balance [78]. Moreover, the enrichment of apoptotic process in HGA-treated sample in comparison with CTR was also confirmed by the up-regulation of BCL2L13, BCLAF1 and CYSC. The interaction network of the above-described proteins and pathways are shown in Fig. 10.

In conclusion, shotgun proteomics confirmed the finding of C20 autophagic, apoptotic and mitochondrial long-term response to HGA stimulus.

In order to confirm the proteomic results, wester blotting analysis were performed for Cytochrome C, NDUFV1 and BCL2. Results are re- ported in Fig. 11.

4. Discussion

Autophagy is a fundamental homeostasis mechanism for the turnover of cytosolic components and for the elimination of damaged organelles [22]. Especially in articular cartilage, in which cells have a low rate of turnover, autophagy assumes an important role for cell survival and activity [23]. Alteration of the autophagy process in chondrocytes is an important characteristic in the development of osteoarticular pathology, e.g. osteoarthritis (OA). AKU, for its similarity to osteoarticular diseases such as OA, could be characterized by an alteration of the autophagic processes leading to a progressive loss of cell function and damage of osteoarticular tissues. AKU chondrocytes undergo continuously to HGA influence, which accumulates in cartilage tissues during the disease, causing morphological and functional alteration of cells [10, 44]. Moreover, we previously found that in AKU and HGA-treated chondrocytes an over activation of the Hedgehog pathway occurs [17, 18] that is known to inhibit autophagy by blocking the autophagosome synthesis [45], thus supporting the hypothesis of an alteration of autophagy. In the present study, we used a chondrocytic model, based on C20 chondrocytic cell line, in order to evaluate the HGA effect on the autophagic activity by the quantification of the expression of LC3-II and of the number of LC3-II puncta.

Autophagy is the first line of defense against different types of stress and occurs at the first steps of the damage, therefore the increased levels of autophagy that was observed after short term HGA treatment in C20 cells, would probably act as a defensive protection against the numerous stresses HGA has reported to be able to induce [5,13,16]. The analysis of autophagy showed an increased level of LC3-II and of autophagosomes after HGA treatment, confirming its role as inducer and enhancer of short-term autophagy. It has been shown that HGA can indirectly alter the cell protein folding machinery [44] by reducing the amount of chaperones, like alpha-crystallin B chain (CRYAB) [15], and by carbonylation

of proteins involved in folding, like GRP75 and HSP7C [15]. Therefore, the increase in the autophagy with the HGA action could be a response mechanism implemented by cells for the elimination of malfunctioning proteins.

Table 1
Down and up-regulated proteins, in HGA-treated cells, involved in autophagy, mitochondrial damage and apoptosis.

Uniprot-Accession	Description	Gene official symbol	Fold change	up/down regulation IN HGA-TrEATED SAMPLE
A6NCE7	Microtubule-associated proteins 1A/1B light chain 3 beta 2	MAP1LC3B2 or LC3-II	0,32	down regulated
O95721	Synaptosomal-associated protein 29	SNAP29	2,53	up-regulation
P00491	Purine nucleoside phosphorylase	PNP	2,86	up-regulation
P04406	Glyceraldehyde-3-phosphate dehydrogenase	GAPDH	2,04	up-regulation
P06576	ATP synthase subunit beta, mitochondrial	ATP5B	1,73	up-regulation
P30044	Peroxiredoxin-5, mitochondrial	PRDX5	2,14	up-regulation
P49327	Fatty acid synthase	FASN	1,66	up-regulation
P61604	10 kDa heat shock protein, mitochondrial	HSPE1	2,10	up-regulation
P62195	26S protease regulatory subunit 8	PSMC5	2,37	up-regulation
Q06830	Peroxiredoxin-1	PRDX1	1,97	up-regulation
Q13423	NAD(P) transhydrogenase, mitochondrial	NNT	1,51	up-regulation
Q92520	Protein FAM3C	FAM3C	2,54	up-regulation
P49821	NADH dehydrogenase [ubiquinone] flavoprotein 1, mitochondrial	NDUFV1	1,64	up-regulation
Q9BXK5	Bcl-2-like protein 13	BCL2L13	5,57	up-regulation
Q9NYF8	Bcl-2-associated transcription factor 1	BCLAF1	2,46	up-regulation
P99999	Cytochrome c	CYCS	3,54	up-regulation

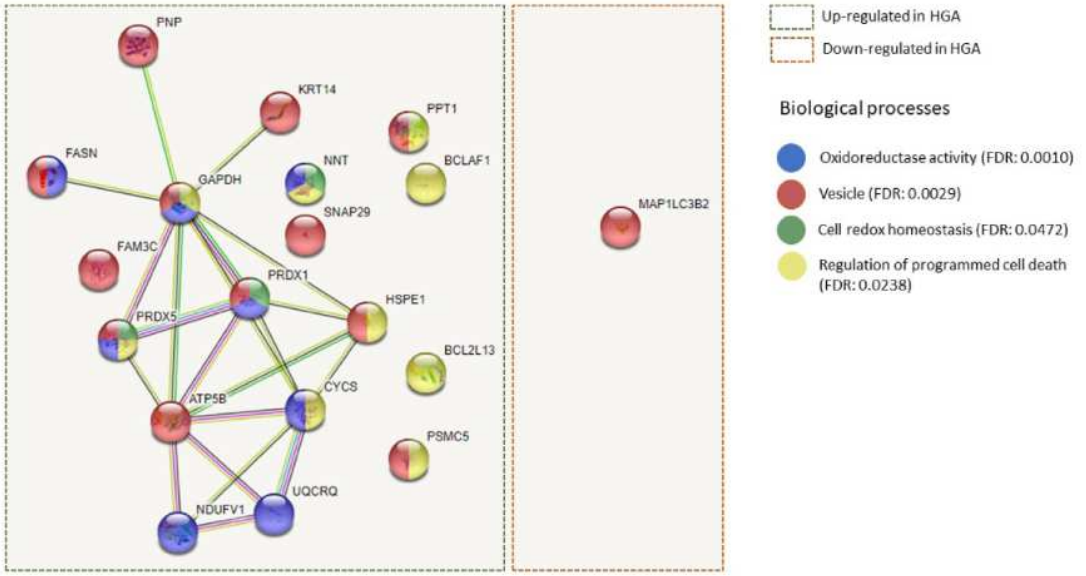

Fig. 10. Specific interaction networks and enrichment analysis on differentially expressed proteins. It is also shown the list of associated pathways with related p-value (<0.05).

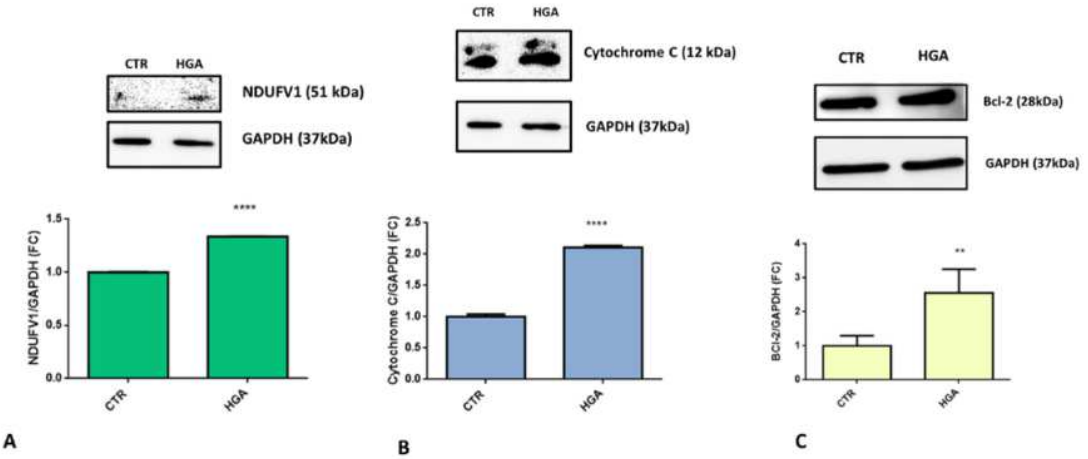

Fig. 11. Increasing of NDUFV1 (panel A), Cytochrome C (panel B), BCL-2 (panel C) expression after HGA treatment. The ratio between band volume of Cytochrome C, NDUFV1 and BCL2 over band volume of GAPDH is reported in fold change.

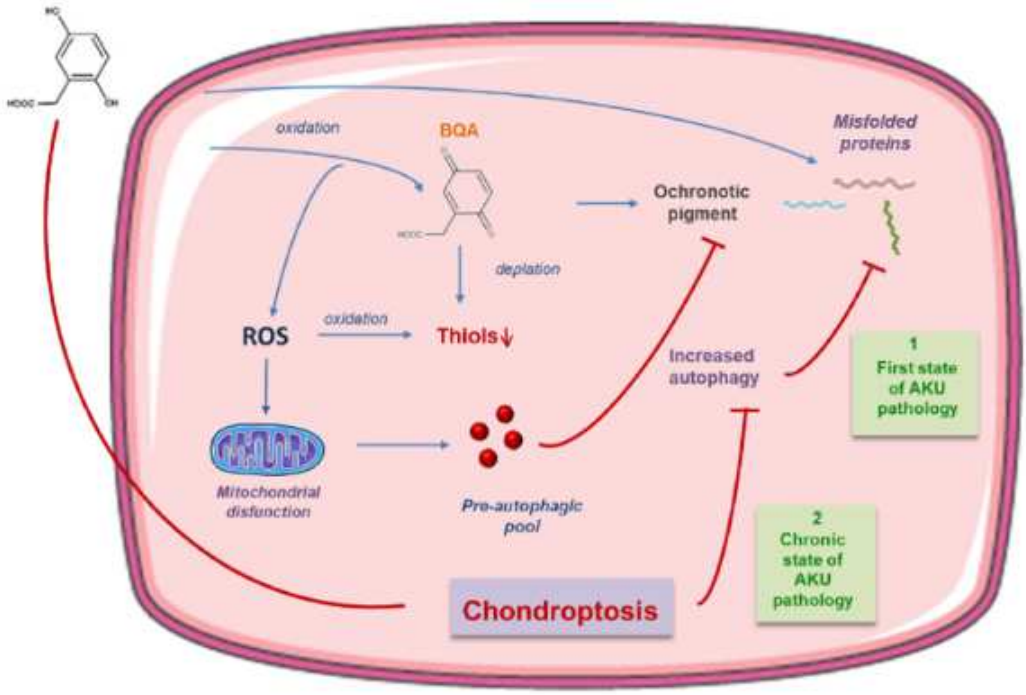

Fig. 12. Mechanism proposed to contribute to autophagy alteration and pigment deposition caused by HGA accumulation.

When C20 cells were submitted to prolonged stress caused by HGA (until 2weeks) the decrease in the autophagy was evident. The stress caused by HGA for longer time implied that cells lost the ability to long term damage by the activation of autophagy and probably the defense pathways failed. The decrease of this protective mechanism, therefore, implicates the loss of cellular homeostasis and of cytoprotective effects and maybe responsible of the reported devastating cell and tissue damages typical of cartilage destruction, reported in AKU [46]. The decrease of autophagy is also confirmed by the proteomic data that reported a different regulation of some pathways involved in autophagy, such as the mTOR pathway. mTOR plays an important and complex role in the induction or termination of autophagy and its activation leads to the decrease of autophagic processes [47]. Also the activation of the p38 MAPK signaling pathway implicates the down regulation of autophagy and an increase in apoptosis [48,49]. Moreover an important connection between autophagy and p53 pathway is already reported, indeed autophagy suppresses p53 and also p53 activates autophagy [50]. After proteomic analysis an upregulation of p53 pathway was evaluated, validating the hypothesis of a decrease of the autophagic processes after a long HGA treatment.

In recent years, HGA was proved to generate and propagate oxidative stress in great number of AKU models and samples [13,16] causing protein oxidation, carbonylation, misfolding and malfunction. Thiols, important groups for the protection of cells against various endogenous and exogenous stresses [51,52], are very sensitive to oxidative stress, indeed free total thiol levels measurement is largely used to evaluate excess ROS and free radical generation. The HGA action on C20 cells caused the decrease of free total thiols, which corresponds with a concomitant decrease of ROS amount. ROS are probably so low because they react directly with cellular free thiols. Moreover, the HGA oxidation product, benzoquinone acetate (BQA), being a p-benzoquinone, could form adducts with protein thiols, causing their depletion [14] and decreasing the cell ability to counterbalance the oxidative stress.

Also oxidative stress has a role in the decrease of autophagy. Indeed in most cells oxidative stress activate mTOR pathway through some processes of oxidation, concluding with the blocking of autophagy [47]. An alteration of mitochondrial structure was demonstrated in AKU chondrocytes, through TEM analysis, indicating the loss of their important activity. Damaged mitochondria are known to induce a pre-autophagic pool with the formation of new autophagosomes, causing the stabilization of the autophagic response to oxidative stress [53]. In a state of continuous stress, cells lose the ability to response to long term damage by the activation of autophagy and the defense pathways fail leading to a specific type of cell death that occurs in AKU chondrocytes, chondroptosis. The caspase involvement, convoluted nuclei and the presence of autophagic vacuoles are some of the characteristics of chondroptosis [54,55], which is common in other articular disease, such as OA [54,56]. Interestingly, we showed that HGA induces chondroptosis on our model, confirming what seen in AKU primary chondrocytes [19]. The activation of apoptotic events in cells treated with HGA was confirmed with proteomic analysis, where we see an increase of BCL2L13 and BCLAF1, which can promote the activation of caspase-3 [57] and, therefore, apoptosis. Indeed, the activation of pro-apoptotic members of the Bcl-2 family leads to altered mitochondrial membrane permeability resulting in release of CYSC into the cytosol [58]. Binding of CYSC to Apaf-1 triggers the activation of caspase-9, which then accelerates apoptosis by activating other caspases [59].

Here we show that autophagy, at early stage of the damage, could be activated as a response to avoid cell death and this process could act together with apoptosis. At the last phase, autophagic processes give way to cellular death, which would recapitulate the cartilage damage seen in AKU patients and the overall progression of AKU pathology (Fig. 12). These new findings and information will be integrated in ApreciseKUre, an AKU-dedicated digital platform where all the biochemical, genetic clinical information, images and data regarding AKU pathophysiology are collected and analyzed with the aim to promote a better understanding of molecular mechanisms and signaling pathways in AKU and in other related co-morbidities [60–65].

5. Conclusion

In this study new aspects of the AKU pathology were explored, characterizing the role of HGA in the alteration of autophagic processes. HGA was shown to cause a state of oxidative stress that over time decreases the protective autophagic process, leading the chondrocytes to the irreversible state of cell death, chondroptosis. We speculate that HGA-induced block of autophagy is responsible for the accumulation of ochronotic pigment, characteristic of AKU manifestation.

Funding

This research did not receive any specific grant from funding agencies in the public, commercial, or not-for-profit sectors.

Author contributions

S. Galderisi, G. Bernardini and A. Santucci contributed to the conception and design of research. S. Galderisi performed the acquisition, collection, analysis and interpretation of data with the contribution of M.S. Milella, M. Rossi, G. Bernardini and A. Santucci.

Experiments for TEM analysis were performed by P. Lupetti. V. Cicaloni carried out proteomic analysis, performing calculations and interpreting data, with the support and supervision of L. Tinti, L. Salvini, and C. Tinti. S. Galderisi wrote the manuscript with support from L. Millucci, D. Braconi, R. Rossi, O. Spiga, D. Giustarini and F. Prischi. The supervision of the work and final approval of the version to be submitted was carried out by A. Santucci.

Declaration of competing interest

The authors declare no conflict of interests.

Acknowledgments

The authors thank the Associazione Italiana Malati di Alcaptonuria (AimAKU; ORPHA263402), DevelopAKUre, DoE 2018–2022 and BiBiM.

Appendix A. Supplementary data

Supplementary data to this article can be found online at https://doi.org/10.1016/j.abb.2022.109137.

References

1. M. Nemethova, J. Radvanszky, L. Kadasi, D.B. Ascher, D.E. Pires, T.L. Blundell, B. Porfirio, A. Mannoni, A. Santucci, L. Milucci, S. Sestini, G. Biolcati, F. Sorge, C. Aurizi, R. Aquaron, M. Alsbou, C. Marques Lourenço, K. Ramadevi, L. R. Ranganath, J.A. Gallagher, C. van Kan, A.K. Hall, B. Olsson, N. Sireau, H. Ayoob, O.G. Timmis, K.H. Le Quan Sang, F. Genovese, R. Imrich, J. Rovensky, R. Srinivasaraghavan, S.K. Bharadwaj, R. Spiegel, A. Zatkova, Twelve novel HGD gene variants identified in 99 alkaptonuria patients: focus on 'black bone disease' n Italy, Eur. J. Hum. Genet. 24 (1) (2016) 66–72, https://doi.org/10.1038/ ejhg.2015.60.

2. Bernini, S. Galderisi, O. Spiga, G. Bernardini, N. Niccolai, F. Manetti, A. Santucci, Toward a generalized computational workflow for exploiting transient pockets as new targets for small molecule stabilizers: application to the homogentisate 1,2-dioxygenase mutants at the base of rare disease Alkaptonuria, Comput. Biol. Chem. 70 (2017) 133–141, https://doi.org/10.1016/j. compbiolchem.2017.08.008.

3. L. Millucci, G. Bernardini, A. Spreafico, M. Orlandini, D. Braconi, M. Laschi, M. Geminiani, P. Lupetti, G. Giorgetti, C. Viti, B. Frediani, B. Marzocchi, A. Santucci, Histological and ultrastructural characterization of alkaptonuric tissues, Calcif. Tissue Int. (2017), https://doi.org/10.1007/s00223-017-0260-9.

4. L. Millucci, L. Ghezzi, E. Paccagnini, G. Giorgetti, C. Viti, D. Braconi, M. Laschi, M. Geminiani, P. Soldani, P. Lupetti, M. Orlandini, C. Benvenuti, F. Perfetto, A. Spreafico, G. Bernardini, A. Santucci, Amyloidosis, inflammation, and oxidative stress in the heart of an alkaptonuric patient, Mediat. Inflamm. (2014), 258471, https://doi.org/10.1155/2014/258471, 2014.

5. L. Millucci, L. Ghezzi, G. Bernardini, D. Braconi, P. Lupetti, F. Perfetto, M. Orlandini, A. Santucci, Diagnosis of secondary amyloidosis in alkaptonuria, Diagn. Pathol. 26 (9) (2014) 185, https://doi.org/10.1186/s13000-014-0185-9.

6. R. Kazancioglu, I. Taylan, F. Aksak, H. Durak, B. Kumbasar, M. Yenigun, F. Sar, Alkaptonuria and renal failure: a case report, J. Nephrol. 17 (3) (2004) 441–445.

7. G. Bernardini, M. Laschi, M. Geminiani, D. Braconi, E. Vannuccini, P. Lupetti, F. Manetti, L. Millucci, A. Santucci, Homogentisate 1,2 dioxygenase is expressed in brain: implications in alkaptonuria, J. Inherit. Metab. Dis. 38 (5) (2015) 807–814, https://doi.org/10.1007/s10545-015-9829-5.

8. M. Laschi, L. Tinti, D. Braconi, L. Millucci, L. Ghezzi, L. Amato, E. Selvi, A. Spreafico, G. Bernardini, A. Santucci, Homogentisate 1,2 dioxygenase is expressed in human osteoarticular cells: implications in alkaptonuria, J. Cell. Physiol. 227 (9) (2012) 3254–3257, https://doi.org/10.1002/jcp.24018.

9. M. Geminiani, S. Gambassi, L. Millucci, P. Lupetti, G. Collodel, L. Mazzi, B. Frediani, D. Braconi, B. Marzocchi, M. Laschi, G. Bernardini, A. Santucci, Cytoskeleton aberrations in alkaptonuric chondrocytes, J. Cell. Physiol. 232 (7) (2017) 1728–1738, https://doi.org/10.1002/jcp.25500.

10. L. Millucci, L. Ghezzi, G. Bernardini, D. Braconi, P. Lupetti, F. Perfetto, M. Orlandini, A. Santucci, Diagnosis of secondary amyloidosis in alkaptonuria, Diagn. Pathol. 26 (9) (2014) 185, https://doi.org/10.1186/s13000-014-0185-9.

11. V. Cicaloni, O. Spiga, G.M. Dimitri, R. Maiocchi, L. Millucci, D. Giustarini, G. Bernardini, A. Bernini, B. Marzocchi, D. Braconi, A. Santucci, Interactive alkaptonuria database: investigating clinical data to improve patient care in a rare disease, Faseb. J. 33 (11) (2019) 12696–12703.

12. L. Millucci, G. Bernardini, B. Marzocchi, D. Braconi, M. Geminiani, S. Gambassi, M. Laschi, B. Frediani, F. Galvagni, M. Orlandini, A. Santucci, Angiogenesis in alkaptonuria, J. Inherit. Metab. Dis. 39 (6) (2016) 801–806, https://doi.org/10.1007/s10545-016-9976-3.

13. D. Braconi, L. Millucci, G. Bernardini, A. Santucci, Oxidative stress and mechanisms of ochronosis in alkaptonuria, Free Radic. Biol. Med. 88 (2015) 70–80, https://doi.org/10.1016/j.freeradbiomed.2015.02.021.

14. D. Braconi, C. Bianchini, G. Bernardini, M. Laschi, L. Millucci, A. Spreafico, A. Santuccim, Redox-proteomics of the effects of homogentisic acid in an in vitro human serum model of alkaptonuric ochronosis, J. Inherit. Metab. Dis. 34 (6) (2011) 1163–1176, https://doi.org/10.1007/s10545-011-9377-6.

15. D. Braconi, M. Laschi, A.M. Taylor, G. Bernardini, A. Spreafico, L. Tinti, J. A. Gallagher, A. Santucci, Proteomic and redox-proteomic evaluation of homogentisic acid and ascorbic acid effects on human articular chondrocytes, J. Cell. Biochem. 111 (4) (2010) 922–932, https://doi.org/10.1002/jcb.22780.

16. D. Braconi, G. Bernardini, A. Paffetti, L. Millucci, M. Geminiani, M. Laschi, B. Frediani, B. Marzocchi, A. Santucci, Comparative proteomics in alkaptonuria provides insights into inflammation and oxidative stress, Int. J. Biochem. Cell Biol. 81 (Pt B) (2016) 271–280, https://doi.org/10.1016/j.biocel.2016.08.016.

17. S. Gambassi, M. Geminiani, S.D. Thorpe, G. Bernardini, L. Millucci, D. Braconi, M. Orlandini, C.L. Thompson, E. Petricci, F. Manetti, M. Taddei, M.M. Knight, A. Santucci, Smoothened-antagonists reverse homogentisic acid-induced alterations of Hedgehog signaling and primary cilium length in alkaptonuria, J. Cell. Physiol. 232 (11) (2017) 3103–3111, https://doi.org/10.1002/jcp.25761.

18. Thorpe, S.D., Gambassi, S., Thompson, C.L., Chandrakumar, C., Santucci, A., Knight, M.M. (2107). Reduced Primary Cilia Length and Altered Arl13b Expression Are Associated with Deregulated Chondrocyte Hedgehog Signalling in Alkaptonuria. J Cell Physiol, 232(9):2407-2417. DOI: 10.1002/jcp.25839.

19. L. Millucci, G. Giorgetti, C. Viti, L. Ghezzi, S. Gambassi, D. Braconi, B. Marzocchi, A. Paffetti, P. Lupetti, G. Bernardini, M. Orlandini, A. Santucci, Chondroptosis in alkaptonuric cartilage, J. Cell. Physiol. 230 (5) (2015) 1148–1157, https://doi.org/10.1002/jcp.24850.

20. L. Millucci, A. Spreafico, L. Tinti, D. Braconi, L. Ghezzi, E. Paccagnini, G. Bernardini, L. Amato, M. Laschi, E. Selvi, M. Galeazzi, A. Mannoni, M. Benucci, P. Lupetti, F. Chellini, M. Orlandini, A. Santucci, Alkaptonuria is a novel human secondary amyloidogenic disease, Biochim. Biophys. Acta 1822 (11) (2012) 1682–1691, https://doi.org/10.1016/j.bbadis.2012.07.011.

21. B. Caramés, N. Taniguchi, S. Otsuki, F.J. Blanco, M. Lotz, Autophagy is a protective mechanism in normal cartilage and its aging-related loss is linked with cell death and osteoarthritis, Arthritis Rheum. 62 (3) (2010) 791–801, https://doi.org/10.1002/art.27305.

22. D. Glick, S. Barth, K.F. Macleod, Autophagy: cellular and molecular mechanisms, J. Pathol. 221 (1) (2010) 3–12, https://doi.org/10.1002/path.2697.

23. M.B. Goldring, S.R. Goldring, Osteoarthritis, J. Cell. Physiol. 213 (3) (2007) 626–634, https://doi.org/10.1002/jcp.21258.

24. A.M. Cuervo, E. Bergamini, U.T. Brunk, W. Dröge, M. Ffrench, A. Terman, Autophagy and aging: the importance of maintaining "clean" cells, Autophagy 1 (3) (2005) 131–140, https://doi.org/10.4161/auto.1.3.2017.

25. H. Jeon, G. Im, Autophagy in osteoarthritis, Connect. Tissue Res. 58 (6) (2017) 497–508, https://doi.org/10.1080/03008207.2016.1240790.

28. D. Braconi, M. Laschi, L. Amato, G. Bernardini, L. Millucci, R. Marcolongo, G. Cavallo, A. Spreafico, A. Santucci, Evaluation of anti-oxidant treatments in an in vitro model of alkaptonuric ochronosis, Rheumatology 49 (2010) 1975–1983, https://doi.org/10.1093/rheumatology/keq175.

29. L. Tinti, A.M. Taylor, A. Santucci, B. Wlodarski, P.J. Wilson, J.C. Jarvis, W. D. Fraser, J.S. Davidson, L.R. Ranganath, J.A. Gallagher, Development of an in vitro model to investigate joint ochronosis in alkaptonuria, Rheumatology 50 (2) (2011) 271–277, https://doi.org/10.1093/rheumatology/keq246.

30. N.B. Roberts, S.A. Curtis, A.M. Milan, L.R. Ranganath, The pigment in alkaptonuria relationship to melanin and other coloured substances: a review of metabolism, composition and chemical analysis, JIMD Rep 24 (2015) 51–66, https://doi.org/10.1007/8904_2015_453.

31. A.J. Preston, C.M. Keenan1, H. Sutherland, P.J. Wilson, B. Wlodarski, A.M. Taylor, D.P. Williams, L.R. Ranganath, J.A. Gallagher, G.C. Jarvis, Ochronotic osteoarthropathy in a mouse model of alkaptonuria, and its inhibition by nitisinone, Ann. Rheum. Dis. 73 (1) (2014) 284–289, https://doi.org/10.1136/annrheumdis-2012-202878.

32. H. Hara, M. Naito, T. Harada, I. Tsuboi, T. Terui, S. Aizawa, Quantitative analysis of formaldehyde-induced fluorescence in paraffin-embedded specimens of malignant melanomas and other melanocytic lesions, Acta Derm. Venereol. 96 (3) (2016) 309–313, https://doi.org/10.2340/00015555-2238.

33. J.R. Wisniewski, A. Zougman, N. Nagaraj, M. Mann, Universal sample preparation method for proteome analysis, Nat. Methods (2009) 359–362, https://doi.org/10.1038/nmeth.1322.

34. W. Huang da, B.T. Sherman, R.A. Lempicki, Bioinformatics enrichment tools: paths toward the comprehensive functional analysis of large gene lists, Nucleic Acids Res. 37 (1) (2008) 1–13, https://doi.org/10.1093/nar/gkn923.

35. M. Pathan, S. Keerthikumar, D. Chisanga, R. Alessandro, C.S. Ang, P. Askenase, A. O. Batagov, A. Benito-Martin, G. Camussi, A. Clayton, F. Collino, D. Di Vizio, J. M. Falcon-Perez, P. Fonseca, P. Fonseka, S. Fontana, Y.S. Gho, A. Hendrix, E. Nolte-'t Hoen, N. Iraci, K. Kastaniegaard, T. Kislinger, J. Kowal, I.V. Kurochkin, T. Leonardi, Y. Liang, A. Llorente, T.R. Lunavat, S. Maji, F. Monteleone, A. Overbye, T. Panaretakis, T. Patel, H. Peinado, S. Pluchino, S. Principe, G. Ronquist, F. Royo, S. Sahoo, C. Spinelli, A. Stensballe, C. Thery, M. van Herwijnen, M. Wauben, J. Welton, J. Zhao, S.J. Mathivanan, A novel community driven software for functional enrichment analysis of extracellular vesicles data, Extracell Vesicles 6 (1) (2017), 1321455, https://doi.org/10.1080/20013078.2017.1321455, 26.

36. M. Ashburner, C.A. Ball, J.A. Blake, D. Botstein, H. Butler, J.M. Cherry, A.P. Davis, K. Dolinski, S.S. Dwight, J.T. Eppig, Gene ontology: tool for the unification of biology. The Gene Ontology Consortium, Nat. Genet. 25 (1) (2000) 25–29, https://doi.org/10.1038/75556.

37. S. Yon Rhee, V. Wood, K. Dolinski, S. Draghici, Use and misuse of the geneontology annotations, Nat. Rev. Genet. 9 (7) (2008) 509–515, https://doi.org/10.1038/nrg2363.

38. Y. Ishihama, Y. Oda, T. Tabata, T. Sato, T. Nagasu, J. Rappsilber, M. Mann, Exponentially Modified Protein Abundance Index (emPAI) for Estimation of absolute protein amount in proteomics by the number of sequenced peptides per protein, Mol. Cell. Proteomics 4 (9) (2005) 1265–1272, https://doi.org/10.1074/mcp.M500061-MCP200.

39. J. Roy, K.L. Wycislo, H. Pondenis, T.M. Fan, A. Das, Comparative proteomics investigation of metastatic and non-metastatic osteosarcoma cells of human and canine origin, PLoS One 12 (9) (2017), e0183930, https://doi.org/10.1371/journal.pone.0183930, 14.

40. J.B. Mistry, D.J. Jackson, M. Bukhari, A.M. Taylor, A role for interleukins in ochronosis in a chondrocyte in vitro model of alkaptonuria, Clin. Rheumatol. 35 (2016) 1849–1856, https://doi.org/10.1007/s10067-015-3091-y.

41. N. Mizushima, T. Yoshimori, B. Levine, Methods in mammalian autophagy research, Cell 140 (3) (2010) 313–326, https://doi.org/10.1016/j.cell.2010.01.028, 5.

42. C. Vinatier, E. Domínguez, J. Guicheux, B. Caram´es, Role of the inflammation- autophagy-senescence integrative network in osteoarthritis, Front. Physiol. 9 (2018), 706, https://doi.org/10.3389/fphys.2018.00706.

43. C. Ruiz-Romero, V. Calamia, J. Mateos, V. Carreira, M. Martínez-Gomariz, M. Fern´andez, F.J. Blanco, Mitochondrial dysregulation of osteoarthritic human articular chondrocytes analyzed by proteomics: a decrease in mitochondrial superoxide dismutase points to a redox imbalance, Mol. Cell. Proteomics 8 (1) (2009) 172–189, https://doi.org/10.1074/mcp.M800292-MCP200.

44. D. Braconi, G. Bernardini, C. Bianchini, M. Laschi, L. Millucci, L. Amato, L. Tinti, T. Serchi, F. Chellini, A. Spreafico, A. Santucci, Biochemical and proteomic characterization of alkaptonuric chondrocytes, J. Cell. Physiol. 227 (9) (2012) 3333–3343, https://doi.org/10.1002/jcp.24033.

45. M. Jimenez-Sanchez, F.M. Menzies, Y.Y. Chang, N. Simecek, T.P. Neufeld, D. C. Rubinsztein, The Hedgehog signalling pathway regulates autophagy, Nat. Commun. 3 (2012) 1200, https://doi.org/10.1038/ncomms2212.

46. G. Bernardini, G. Leone, L. Millucci, M. Consumi, D. Braconi, O. Spiga, S. Galderisi, B. Marzocchi, C. Viti, G. Giorgetti, P. Lupetti, A. Magnani, A. Santucci, Homogentisic acid induces morphological and mechanical aberration of ochronotic cartilage in alkaptonuria, J. Cell. Physiol. (2018), https://doi.org/10.1002/jcp.27416

47. A. Perl, Activation of mTOR (mechanistic target of rapamycin) in rheumatic diseases, Nat. Rev. Rheumatol. 12 (3) (2016) 169–182, https://doi.org/10.1038/nrrheum.2015.172.

48. J. Shi, C. Zhang, Z. Yi, C. Lan, Explore the variation of MMP3, JNK, p38 MAPKs, and autophagy at the early stage of osteoarthritis, IUBMB Life 68 (4) (2016) 293–302, https://doi.org/10.1002/iub.1482.

49. H.Y. Sun, K.Z. Hu, Z.S. Yin, Inhibition of the p38-MAPK signaling pathway suppresses the apoptosis and expression of proinflammatory cytokines in human osteoarthritis chondrocytes, Cytokine 90 (2017) 135–143, https://doi.org/10.1016/j.cyto.2016.11.002.

50. E. White, Autophagy and p53, Cold Spring Harb Perspect Med 6 (4) (2016), a026120, https://doi.org/10.1101/cshperspect.a026120, 1.

51. M. Wang, Q. Zhao, W. Liu, The versatile low-molecular-weight thiols: beyond cell protection, Bioessays 37 (12) (2015) 1262–1267, https://doi.org/10.1002/bies.201500067.

52. M.E. Murphy, H. Scholich, H. Sies, Protection by glutathione and other thiol compounds against the loss of protein thiols and tocopherol homologs during microsomal lipid peroxidation, Eur. J. Biochem. 210 (1) (1992) 139–146.

53. Goutas, C. Syrrou, I. Papathanasiou, A. Tsezou, V. Trachana, The autophagic response to oxidative stress in osteoarthritic chondrocytes is deregulated, Free Radic. Biol. Med. 126 (2018) 122–132, https://doi.org/10.1016/j.freeradbiomed.2018.08.003.

54. E. Charlier, B. Relic, C. Deroyer, O. Malaise, S. Neuville, J. Coll´ee, M.G. Malaise, D. De Seny, Insights on molecular mechanisms of chondrocytes death in osteoarthritis, Int. J. Mol. Sci. 17 (12) (2016), 2146, https://doi.org/10.3390/ijms17122146.

55. H.I. Roach, T. Aigner, J.B. Kouri, Chondroptosis: a variant of apoptotic cell death in chondrocytes? Apoptosis 9 (3) (2004) 265–277, https://doi.org/10.1023/b:appt.0000025803.17498.26.

56. H.E. Pérez, M.J. Luna, M.L. Rojas, J.B. Kouri, Chondroptosis: an immunohistochemical study of apoptosis and Golgi complex in chondrocytes from human osteoarthritic cartilage, Apoptosis 10 (5) (2005) 1105–1110, https://doi.org/10.1007/s10495-005-0649-1.

57. E. Swanton, P. Savory, S. Cosulich, P. Clarke, P. Woodman, Bcl-2 regulates a caspase-3/caspase-2 apoptotic cascade in cytosolic extracts, Oncogene 18 (1999) 1781–1787.

58. J.E. Chipuk, D.R. Green, How do BCL-2 proteins induce mitochondrial outer membrane permeabilization? Trends Cell Biol. 18 (4) (2008) 157–164, https://doi.org/10.1016/j.tcb.2008.01.007.

59. X. Jiang, X. Wang, Cytochrome C promotes caspase-9 activation by inducing nucleotide binding to apaf-1, J. Biol. Chem. 275 (40) (2000) 31199–31203, https://doi.org/10.1074/jbc.C000405200.

60. V. Cicaloni, O. Spiga, G.M. Dimitri, R. Maiocchi, L. Millucci, D. Giustarini, G. Bernardini, A. Bernini, B. Marzocchi, D. Braconi, A. Santucci, Interactive alkaptonuria database: investigating clinical data to improve patient care in a rare disease, Faseb. J. 33 (11) (2019) 12696–12703, https://doi.org/10.1096/fj.201901529R.

61. O. Spiga, V. Cicaloni, A. Zatkova, L. Millucci, G. Bernardini, A. Bernini, B. Marzocchi, M. Bianchini, A. Zugarini, A. Rossi, M. Zazzeri, A. Trezza, B. Frediani, L. Ranganath, D. Braconi, A. Santucci, A new integrated and interactive tool applicable to inborn errors of metabolism: application to alkaptonuria, Comput. Biol. Med. 103 (2018) 1–7, https://doi.org/10.1016/j.compbiomed.2018.10.002.

62. O. Spiga, V. Cicaloni, A. Bernini, A. Zatkova, A. Santucci, ApreciseKUre: an approach of precision medicine in a rare disease, BMC Med. Inf. Decis. Making 17 (2017) 42, https://doi.org/10.1186/s12911-017-0438-0.

63. V. Cicaloni, A. Zugarini, A. Rossi, M. Zazzeri, A. Santucci, A. Bernini, O. Spiga, Towards an integrated interactive database for the search of stratification biomarkers in Alkaptonuria, PeerJ Preprints 4 (2016), e2174v1, https://doi.org/10.7287/peerj.preprints.2174v.

64. O. Spiga, V. Cicaloni, C. Fiorini, A. Trezza, A. Visibelli, L. Millucci, G. Bernardini, A. Bernini, B. Marzocchi, D. Braconi, F. Prischi, Machine learning application for development of a data-driven predictive model able to investigate quality of life scores in a rare disease, Orphanet J. Rare Dis. 15 (1) (2020) 1, https://doi.org/10.1186/s13023-020-1305-0, 0.

65. Rossi, G. Giacomini, V. Cicaloni, S. Galderisi, M.S. Milella, A. Bernini, L. Millucci, O. Spiga, M. Bianchini, A. Santucci, AKUImg: a database of cartilage images of Alkaptonuria patients, Comput. Biol. Med. 18 (2020), 103863.

66. G.Y. Kang, J.Y. Bang, A.J. Choi, J. Yoon, W.C. Lee, S. Choi, S. Yoon, H.C. Kim, J. H. Baek, H.S. Park, H.J. Lim, H. Chung, Exosomal proteins in the aqueous humor as novel biomarkers in patients with neovascular age-related macular degeneration, J. Proteome Res. 13 (2) (2014) 581–595, https://doi.org/10.1021/pr400751k.

67. M. Sardiello, M. Palmieri, A. di Ronza, D.L. Medina, M. Valenza, V.A. Gennarino, C. Di Malta, F. Donaudy, V. Embrione, R.S. Polishchuk, S. Banfi, G. Parenti, E. Cattaneo, A. Ballabio, A gene network regulating lysosomal biogenesis and function, Science 325 (5939) (2009) 473–477, https://doi.org/10.1126/science.1174447.

68. C. Settembre, C. Di Malta, V.A. Polito, M. Garcia Arencibia, F. Vetrini, S. Erdin, S. U. Erdin, T. Huynh, D. Medina, P. Colella, M. Sardiello, D.C. Rubinsztein, A. Ballabio, TFEB links autophagy to lysosomal biogenesis, Science 332 (6036) (2011) 1429–1433, https://doi.org/10.1126/science.1204592.

69. C. Settembre, A. Fraldi, D.L. Medina, A. Ballabio, Signals from the lysosome: a control centre for cellular clearance and energy metabolism, Nat. Rev. Mol. Cell Biol. 14 (5) (2013) 283–296, https://doi.org/10.1038/nrm3565.

70. E.K. Cudjoe Jr., T. Saleh, A.M. Hawkridge, D.A. Gewirtz, Proteomics insights into autophagy, Proteomics 17 (20) (2017), https://doi.org/10.1002/pmic.201700022.

71. J. Wang, J. Zhang, Y.M. Lee, et al., Quantitative chemical proteomics profiling of de novo protein synthesis during starvation-mediated autophagy, Autophagy 12 (10) (2016) 1931–1944, https://doi.org/10.1080/15548627.2016.1196317.

72. R. Mathew, S. Khor, S.R. Hackett, J.D. Rabinowitz, D.H. Perlman, E. White, Functional role of autophagy-mediated proteome remodeling in cell survival signaling and innate immunity, Mol. Cell. 55 (6) (2014) 916–930, https://doi.org/10.1016/j.molcel.2014.07.019.

73. V. Mastrodonato, E. Morelli, T. Vaccari, How to use a multipurpose SNARE: the emerging role of Snap29 in cellular health, Cell Stress 2 (4) (2018) 72–81, https://doi.org/10.15698/cst2018.04.130.

74. G. Butera, N. Mullappilly, F. Masetto, et al., Regulation of autophagy by nuclear GAPDH and its aggregates in cancer and neurodegenerative disorders, Int. J. Mol. Sci. 20 (9) (2019), 2062, https://doi.org/10.3390/ijms20092062.

75. J.Y. Zhang, F. Zhang, C.Q. Hong, et al., Critical protein GAPDH and its regulatory mechanisms in cancer cells, Cancer Biol Med 12 (1) (2015) 10–22, https://doi.org/10.7497/j.issn.2095-3941.2014.0019.

76. S.W. Kang, H.Z. Chae, M.S. Seo, K. Kim, I.C. Baines, S.G. Rhee, Mammalian peroxiredoxin isoforms can reduce hydrogen peroxide generated in response to growth factors and tumor necrosis factor-alpha, J. Biol. Chem. 273 (11) (1998) 6297–6302, https://doi.org/10.1074/jbc.273.11.6297.

77. K.M. Kober, A. Olshen, Y.P. Conley, et al., Expression of mitochondrial dysfunction-related genes and pathways in paclitaxel-induced peripheral neuropathy in breast cancer survivors, Mol. Pain 14 (2018), 1744806918816462, https://doi.org/10.1177/1744806918816462.

78. K.N.S. Rao, X. Shen, S. Pardue, D.M. Krzywanski, Nicotinamide nucleotide transhydrogenase (NNT) regulates mitochondrial ROS and endothelial dysfunction in response to angiotensin II, Redox Biol. 36 (2020), 101650, https://doi.org/10.1016/j.redox.2020.101650.

79. K. Taniguchi, S. Yamachika, F. He, M. Karin, p62/SQSTM1-Dr. Jekyll and Mr. Hyde that prevents oxidative stress but promotes liver cancer, FEBS Lett. 590 (15) (2016) 2375–2397, https://doi.org/10.1002/1873-3468.12301.

80. B. Carroll, E.G. Otten, D. Manni, R. Stefanatos, F.M. Menzies, G.R. Smith, D. Jurk, N. Kenneth, S. Wilkinson, J.F. Passos, J. Attems, E.A. Veal, E. Teyssou, D. Seilhean, S. Millecamps, E.L. Eskelinen, A.K. Bronowska, D.C. Rubinsztein, A. Sanz, V. I. Korolchuk, Oxidation of SQSTM1/p62 mediates the link between redox state and protein homeostasis, Nat. Commun. 9 (1) (2018) 256, https://doi.org/10.1038/s41467-017-02746-z. PMID: 29343728; PMCID: PMC5772351.

81. E.G. Otten, R. Stefanatos, B. Carroll, V.I. Korolchuk, Oxidation of p62 as an evolutionary adaptation to promote autophagy in stress conditions, Cell Stress 2 (4) (2018) 91–93, https://doi.org/10.15698/cst2018.04.132. PMID: 31225472; PMCID: PMC6551744.